Chapter 2
Mullite

David J. Duval, Subhash H. Risbud, and James F. Shackelford

Abstract Mullite is the only stable intermediate phase in the alumina–silica system at atmospheric pressure. Although this solid solution phase is commonly found in human-made ceramics, only rarely does it occur as a natural mineral. Yet mullite is a major component of aluminosilicate ceramics and has been found in refractories and pottery dating back millennia. As the understanding of mullite matures, new uses are being found for this ancient material in the areas of electronics and optics, as well as in high temperature structural products. Many of its high temperature properties are superior to those of most other metal oxide compounds, including alumina. The chemical formula for mullite is deceptively simple: $3Al_2O_3{\cdot}2SiO_2$. However, the phase stability, crystallography, and stoichiometry of this material remain controversial. For this reason, research and development of mullite is presented in an historical perspective that may prove useful to engineers and scientists who encounter this material under nonequilibrium conditions in their work. Emphasis is placed on reviewing studies where the primary goal was to create single-phase mullite monoliths with near theoretical density.

1 Introduction

Mullite is a solid solution phase of alumina and silica commonly found in ceramics. Only rarely does mullite occur as a natural mineral. According to introductory remarks made by Schneider and MacKenzie at the conference "Mullite 2000"[1], the geologists Anderson, Wilson, and Tait of the Scottish Branch of His Majesty's Geological Survey discovered the mineral mullite less than a century ago. The trio was collecting mineral specimens from ancient lava flows on the island of Mull off the west coast of Scotland when they chanced upon the first known natural deposit of this ceramic material. The specimens were initially identified as sillimanite, but later classified as mullite.

Being the only stable intermediate phase in the Al_2O_3–SiO_2 system at atmospheric pressure, mullite is one of the most important ceramic materials. Mullite has been fabricated into transparent, translucent, and opaque bulk forms. These materials may have optical and electronic device applications. Mullite's temperature stability and

J.F. Shackelford and R.H. Doremus (eds.), *Ceramic and Glass Materials: Structure, Properties and Processing*.

refractory nature are superior to corundum's in certain high-temperature structural applications. Another characteristic of this aluminosilicate is its temperature-stable defect structure, which may indicate a potential use in fuel cell electrolytes.

In this chapter, developments in the understanding of mullite over the last few decades are reviewed. A discussion of crystal structures and phase stability is presented to provide the reader with an overview of certain characteristics of this material. The next part of this chapter examines the effect of process chemistry on the synthesis and microstructure of mullite. The role of various synthetic methods that are used to modify mullite formation will be discussed, followed by a compilation of selected materials properties.

2 Crystal Structure

The X-ray diffraction pattern of mullite is very similar to that of sillimanite. Sillimanite is a commonly occurring aluminosilicate mineral stable at high pressures with the chemical formula $Al_4Si_2O_{10}$, a 1:1 ratio of silica to alumina.

Roughly speaking, the sillimanite and mullite structures consist of chains of distorted edge-sharing Al–O octahedra at the corners and center of each unit cell running parallel to the *c*-axis. The chains are cross-linked by Si–O and Al–O corner-sharing tetrahedra [2]. Mullite is a solid solution compound with stoichiometries ranging from relatively silica-rich $3Al_2O_3{\cdot}2SiO_2$ (3:2 mullite) to alumina-rich $2Al_2O_3{\cdot}SiO_2$ (2:1 mullite). The structure of mullite is summarized in Table 1. Some authors use the Al/Si ionic ratio when referring to mullite stoichiometry. In this case, 3:2 mullite would have an aluminum/silicon ionic ratio of 3:1. To avoid further confusion and follow the convention most commonly used in the literature, mullite stoichiometry will be based on the alumina/silica molecular ratio. The chemical formula for mullite is often given by $Al_2(Al_{2+2x}Si_{2-2x})O_{10-x}$, where $x = 0$ corresponds to sillimanite, $x = 0.25$ corresponds

Table 1 Wyckoff positions and coordinates of atom sites for the orthorhombic mullite structure with space group Pbam (No. 55)

Lattice parameters	a = 0.75499(3) nm		b = 0.76883(3)nm			c = 0288379(9) nm	
Atom	Al_2	$[Al_2Si_{2-2x}]$	Al_{2x}	O_{2-3x}	O_{2x}	O_4	O_4
Wyckoff position	2a	4h	4h	2d	4h	4h	4g
Coordinate							
x	0	0.1474(6)	0.268(3)	0.5	0.451(5)	0.3566(6)	0.1263(9)
y	0	0.3410(6)	0.207(2)	0.0	0.048(5)	0.4201(6)	0.2216(8)
z	0	0.5	0.5	0.5	0.5	0.5	0.0
Thermal parameter (β)	0.5(1)	0.3(1)	1.2(8)	0.8(1)	0.8(1)	0.8(1)	0.8(1)
Occupancy							
O	1	0.5	0.166(7)	0.5	0.166(7)	1	1
Al		0.334(7)					
Si							

The chemical formula is $Al_2(Al_{2+2x}Si_{2-2x})O_{10-x}$, where $x = 0.33$ and the calculated density is 3.16 g cm^{-3}. From [57]

to 3:2 mullite, and $x = 0.4$ corresponds to 2:1 mullite. Diffusion studies [3] have shown that the following chemical formula is more appropriate even though it is not commonly seen in the literature:

$$\mathrm{Al}^{\mathrm{VI}}_{\left(\frac{4}{3}+\frac{14}{3}x\right)}\left[\mathrm{Al}^{\mathrm{IV}}_{\frac{8}{3}}\mathrm{Si}_2\right]_{(1-x)}\mathrm{O}_{10-x}\square_x \tag{1}$$

The symbol □ denotes an oxygen vacancy. The superscripts VI and IV indicate octahedral and tetrahedral coordination sites, respectively.

With increasing alumina content, Si^{4+} is replaced by Al^{3+} and anion (oxygen) vacancies are created to maintain charge neutrality. Accommodating the structural defects causes significant distortions of the aluminum and silicon polyhedra. In mullite (as opposed to sillimanite), there are three (as opposed to four) tetrahedral "chains" in the unit cell, with a somewhat random distribution for silica and alumina tetrahedra [4]. This results in the necessity for distorted alumina tetrahedra to be arranged in an oxygen-deficient tricluster (three tetrahedra sharing single corner-bridging oxygen). These clusters constitute a distinctive element of mullite's crystal structure [2,5].

Unlike sillimanite, X-ray diffraction patterns of mullite exhibit significant diffuse scattering and possible superlattice reflections. Authors have proposed various models to account for mullite's anomalous scattering using superlattice refinement, atomic site occupancy factor calculation, and correlated vacancy mapping [2,6,7]. Most work suggests that defects tend to cluster or correlate with short-range order along specific crystallographic directions. Lower alumina concentrations result in less directional correlation of oxygen vacancies or more random vacancy distributions. According to Freimann and Rahman [7], oxygen vacancies tend to correlate parallel with the lattice parameter *a*, and to a lesser extent with *b*. The authors suggest their correlation results could be used to interpret thermal expansion behavior of mullites. As a practical matter, the lattice parameter *a* correlates linearly with

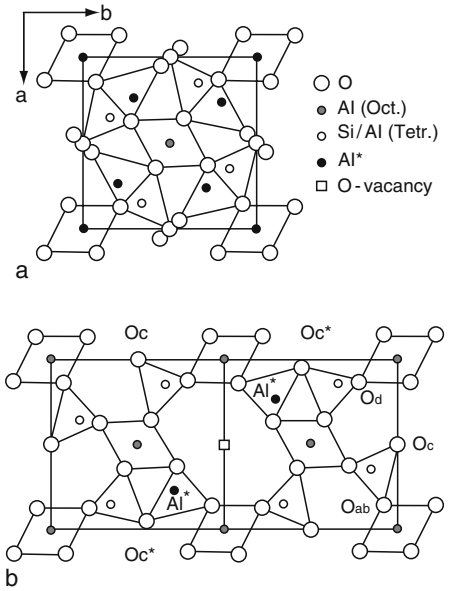

Fig. 1 Structure of mullite. (**a**) Average structure and (**b**) atomic displacements around an oxygen vacancy. From [7]

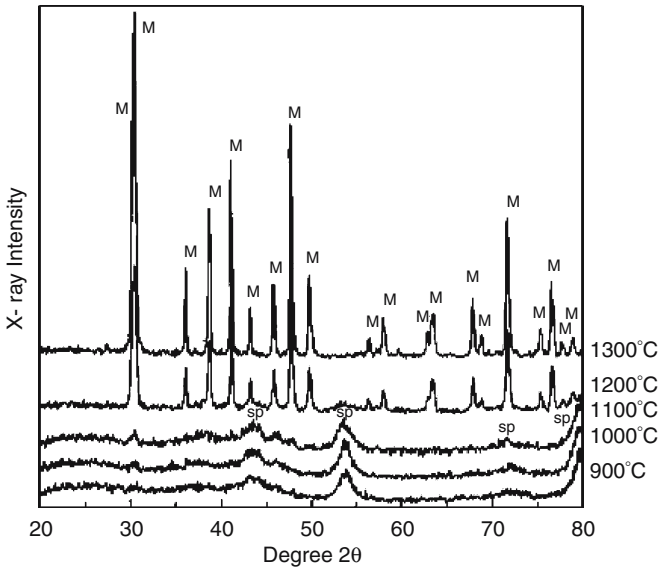

Fig. 2 X-ray powder diffraction patterns showing the crystallization of mullite from amorphous precursors as a function of temperature. M denotes mullite peaks, and Sp markers denote the intermediate γ-Al_2O_3 spinel peaks. From [8]

Al_2O_3 content. Figure 1 depicts the mullite unit. Atom positions for an intermediate composition of mullite, $Al_2(Al_{2+2x}Si_{2-2x})O_{10-x}$, where $x = 0.33$ are provided in Table 1. X-ray powder diffraction patterns demonstrating mullite crystallization from amorphous precursors are shown in Fig. 2 [8].

It should be noted that there is no convincing evidence of mullite formation in regions of the phase diagram with compositions between 3:2 mullite and sillimanite. In other words, the chemical formula for mullite cannot accommodate x values such that $0<x<0.25$. Although the presence of a cubic spinel with the stoichiometry and structure similar to that of 2:1 mullite had been reported [9,10], its existence is likely of academic rather than practical significance. What was originally reported as a tetragonal phase of 3:1 mullite [11] formed by rapid quenching of the melt could be attributed to severe microtwinning of the usual orthorhombic structure [12]. On the other hand, workers have recently reported mullite phases with Al_2O_3/SiO_2 ratios up to and greater than 9:1 [13–15]. These specialty compounds are potentially useful in specific refractory applications due to their high Al_2O_3 content. Unfortunately, it has proved difficult to produce these ultra-high alumina mullites in sufficient quantity and purity. Further research is required before practical applications for these materials can be envisioned.

3 Phase Stability

An historical perspective may prove useful to engineers or scientists who encounter mullite during the course of their work: The earliest interpretations of the material's behavior may reflect the result of nonequilibrium conditions that often occur in production or experimental situations.

Mullite-based ceramics have been widely used as refractories and in pottery for millennia. Although the technology of mullite is becoming more mature, there are still questions concerning its melting behavior and the shape of mullite phase boundaries in the Al_2O_3–SiO_2 phase diagram. In 1924, Bowen and Grieg [16] published the first phase diagram to include mullite as a stable phase, but did not indicate a solid solution range. The phase $3Al_2O_3{\cdot}2SiO_2$ was reported to melt incongruently at 1,810°C. Specimens were prepared from mechanical mixtures of alumina and silica melted and quenched in air. Shears and Archibald [17] reported the presence of a solid solution range from $3Al_2O_3{\cdot}2SiO_2$ (3:2 mullite) to $2Al_2O_3{\cdot}SiO_2$ (2:1 mullite) in 1954. Their phase diagram depicted a mullite solidus shifting to higher alumina concentrations at temperatures above the silica–mullite eutectic temperature.

In 1958, Toropov and Galakhov [18] presented a phase diagram where mullite was shown to melt congruently at 1,850°C. Aramaki and Roy [19] published a phase diagram in 1962 corroborating a congruent melting point for mullite at 1,850°C. Their specimens were prepared from gels for subsolidus heat treatments, while mechanical mixtures of α-Al_2O_3 and silica glass were prepared for heat treatments above the solidus temperature. Specimens were encapsulated to inhibit silica volatilization. A silica–mullite eutectic temperature of 1,595°C and a mullite–alumina eutectic temperature of 1,840°C were reported. No shift in the mullite solidus phase boundary with temperature was reported in either of these publications.

Over a decade later, Aksay and Pask [20] presented a different phase diagram depicting incongruent melting for mullite at 1,828°C. Specimens, in the form of diffusion couples between sapphire and aluminosilicate glass, were also encapsulated to inhibit volatilization. Many authors suggest that nucleation and growth of mullite occurs within an amorphous alumina-rich siliceous phase located between the silica and alumina particles [21–24]. On the other hand, Davis and Pask [25] and later Aksay and Pask observed coherent mullite growth on sapphire in a temperature range from about 1,600 to below 1,800°C, indicating interdiffusion of aluminum and silicon ions through the mullite [20]. Risbud and Pask [26] later modified the diagram to incorporate metastable phase regions. They showed a stable silica–mullite eutectic temperature of 1,587°C. An immiscibility dome with a spinodal region was reported between approximately 7 and 55 mol% Al_2O_3. The dome has a central composition of about 35 mol% Al_2O_3, and complete miscibility occurs near 1,550°C (temperatures below the silica–mullite eutectic temperature). A stable mullite–alumina peritectic was reported at 1,828°C. However, a "metastable" incongruent melting point for mullite was reported at 1,890°C. The "metastable" mullite compositions were shifted toward higher alumina concentration. To account for the metastability, the authors suggested there could be a barrier for alumina precipitation in both melt and mullite, and that mullite could be superheated. Figure 3 portrays this phase diagram showing regions of metastability [27].

In 1987, Klug et al. published their SiO_2–Al_2O_3 phase diagram [28]. They reported incongruent melting for mullite at 1,890°C, and shifting of both boundaries of the mullite solid solution region toward higher alumina content (2:1 mullite) at temperatures above the eutectic point of 1,587°C. This phase diagram appears to reconcile most of the phenomena observed by other workers on the SiO_2–Al_2O_3 system. Seemingly irreconcilable observations involving phase stability of similarly prepared specimens have been attributed convincingly to nonequilibrium conditions and/or silica volatilization. This phase diagram [28] is shown in Fig. 4.

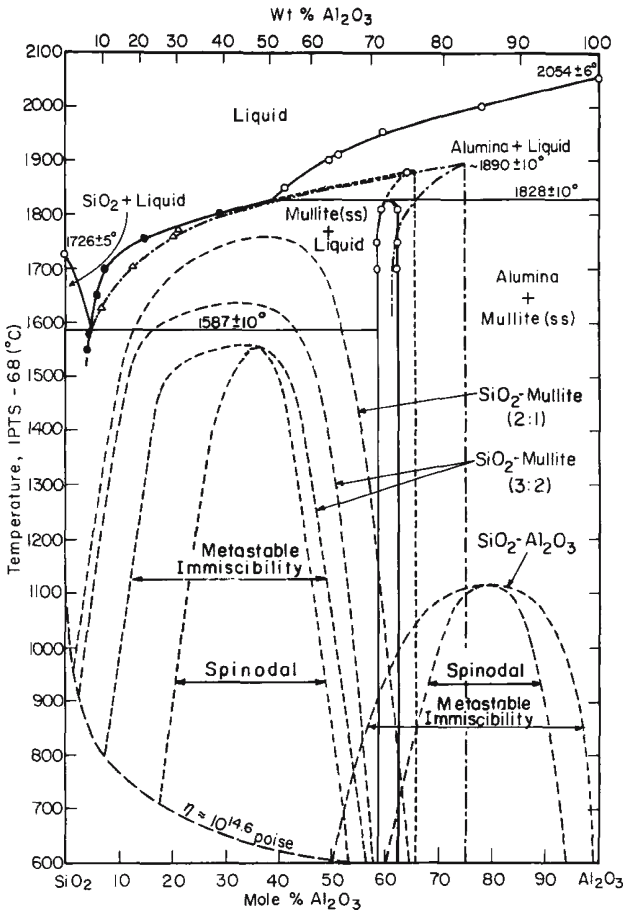

Fig. 3 The system Al_2O_3–SiO_2 showing metastable regions. The gaps shown with spinodal regions are considered the most probable thermodynamically. From [27]

The 2:1 mullite appears to be only metastable at room temperature [28], and very high temperature use or cycling might cause some alumina to precipitate. However, Pask [29] suggested that discrepancies in the reported behavior of mullite are attributable to the presence or absence of α-Al_2O_3 in the starting materials. Engineers or scientists are cautioned to use the appropriate phase diagram consistent with their experimental methods and conditions. It should also be noted that at tectonic pressures, SiO_2 will exsolve from mullite leaving a compound with a stoichiometry $Al_2O_3 \cdot SiO_2$. Depending on temperature and pressure, the compound will be sillimanite, kyanite, or andalusite.

4 Processing and Applications

As mentioned in the previous section, the formation, phase purity, and morphology of mullite depend upon precursor materials and processing history. Mullite was first identified as the product of heating kaolinitic clays, resulting in a compound with an

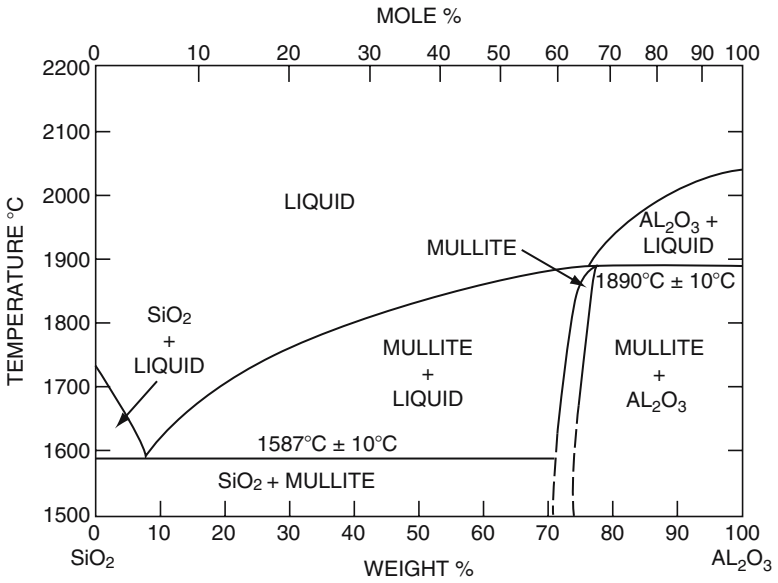

Fig. 4 Phase diagram for the alumina–silica system. From [28]

approximate alumina-to-silica molar ratio of 3:2. The order of reaction proceeds as follows [30]:

$Al_2Si_2O_5(OH)_4$	450°C →	$2(Al_2O_3{\cdot}2SiO_2) + 2H_2O$
Kaolinite		Metakaolin
$2(Al_2O_3{\cdot}2SiO_2)$	925°C →	$2Al_2O_3{\cdot}3SiO_2 + SiO_2$
Metakaolin		Silicon spinel
$2Al_2O_3.3SiO_2$	1,100°C →	$2(Al_2O_3.SiO_2) + SiO_2$
Silicon spinel		Pseudomullite
$3(Al_2O_3.SiO_2)$	1,400°C →	$3Al_2O_3.2SiO_2 + SiO_2$
Pseudomullite		Mullite + cristobalite

Excess corundum may be added, and the system heated at higher temperatures to minimize free SiO_2. Toward this end, Goski and Caley [31] suspended grains of the mineral kyanite (a high-pressure form of $Al_2O_3{\cdot}SiO_2$) with submicron alumina in water to provide intimate mixing of these mullite precursors. The alumina–kyanite suspension was slip cast to form a green body that was reaction-sintered to form an alumina–mullite composite. According to phase diagrams, a silica-rich glassy phase in 3:2 mullite is predicted when sintered at temperatures higher than the eutectic (1,587°C). Many common 3:2 mullite products are sintered between 1,600 and 1,700°C and may contain a glassy phase in the microstructure.

High-purity glass-free mullite monoliths have been obtained by at least three traditional methods:

1. Starting materials with alumina contents near the stoichiometry of 2:1 mullite may be completely melted above 1,960°C and then cooled to about 1,890°C without crystallizing. At the latter temperature (in the shifted solid solution region), infrared-transparent mullite single crystals could be grown by the Czochralski method [32].
2. Pask [29] reports that mullites with higher molar ratios of alumina to silica (i.e., >3:1) have been prepared by homogenous melting of the constituents above the liquids and subsequent quenching. As a note, mullites prepared by fusion are generally weaker than those produced by sintering [33].
3. Mullite powders obtained by various methods can first be crystallized near 1,200°C, and then sintered at temperatures below the eutectic. Highly pure mullite and mullite composites have been obtained by hot pressing below 1,300°C with this method [34].

When processed close to or above the eutectic temperature (~1,590°C), mullite with bulk compositions of less than 72 wt% Al_2O_3 (3:2 mullite) exhibits a microstructure of elongated grains that is believed to be promoted by the presence of a glassy second phase. For Al_2O_3 concentrations greater than 72 wt% Al_2O_3, the amount of glassy phase is less and the initially formed mullite grains are smaller and more equiaxial. Further heat treatment results in rapid grain growth driven by a decrease of the high grain boundary area associated with the fine grains in the initial system. This leads to fast growth of the grains along the *c*-axis and a higher aspect ratio for the overall grains. After this rapid decrease in the driving force, the grains grow more slowly and the overall decrease in the free energy of the system dictates the development of a more equiaxial microstructure [35]

An interesting approach in making mullite powders has been via combustion synthesis [36]. An aqueous heterogeneous redox mixture containing aluminum nitrate, silica fume (soot), and urea in the appropriate mole ratio is mixed together. When rapidly heated to 500°C, the mixture boils, foams, and can be ignited with a flame. The process yields weakly crystalline mullite powder in less than 5 min. Fully crystalline mullite can be obtained by incorporating an extra amount of oxidizer, such as ammonium perchlorate in the solution.

Recent work on mullite synthesis has focused on variations of sol–gel methods, which allow control of the local distribution and homogeneity of the precursor chemistry. The microstructure of a sol–gel derived mullite is shown in Fig. 5. Along with an understanding of kinetics, sol–gel methods look promising for use in the manufacture of bulk materials, thin films, or fibers of mullite with almost any specified phase purity, phase distribution, and grain morphology.

Three categories of gels are usually made [37]. Single-phase (type I) mullite precursor gels have near atomic level homogeneous mixing. The precursors transform into an alumina-rich mullite at about 980°C in the same way as rapidly quenched aluminosilicate glasses. These are formed from the simultaneous hydrolysis of the aluminum and silicon sources. Type I xerogels, for example, can be synthesized from tetraethylorthosilicate (TEOS) or tetramethylorthosilicate (TMOS) and aluminum nitrate nonahydrate [38]. Diphasic (type II) gels comprised two sols with mixing on the nanometer level. These gels, after drying, consist of boehmite and noncrystalline SiO_2, which at ~350°C transform to γ-Al_2O_3 and noncrystalline SiO_2. An example of

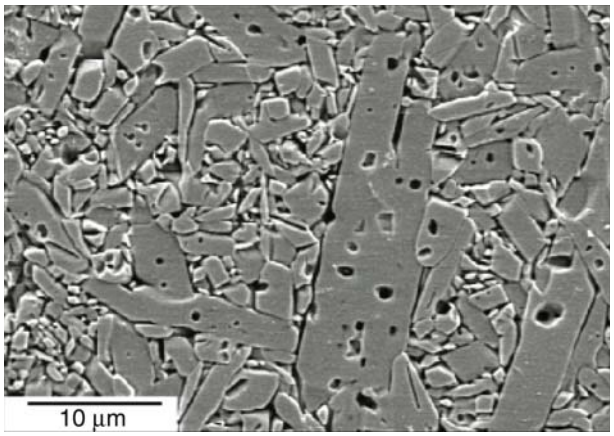

Fig. 5 Scanning electron micrograph of 3:2 mullite. Specimen was sintered at 1,700°C, hot isostatically pressed at 1,600°C, and thermally etched. From [54]

a type II gel would be a mixture of boehmite with a TEOS or TMOS sol [22]. Type III diphasic gels contain precursors that are noncrystalline up to 980°C and then form γ-Al_2O_3 and noncrystalline SiO_2.

Subsequent heat treatments of the three types of gels result in very different microstructures even if the alumina–silica molecular ratios are identical. Mullite conversion from powders or diphasic gels tends to be diffusion rate controlled. In the case of monophasic gels, conversion from the amorphous to crystalline phase appears to be nucleation rate dependent [39]. Such nucleation rate dependence would seem to indicate that it would be difficult to obtain very fine-grained mullite monoliths. However, some researchers have been successful in producing such monoliths. Monophasic xerogels prepared by slow hydrolysis (4–6 months) of hexane solutions of aluminum sec-butoxide and TMOS have been used to make optically clear mullite monoliths. The gel was heated in the range of ~1,000–1,400°C to form a completely dense crystalline material with glass-like mechanical properties (brittle and conchoidal fractures, rapid crack propagation, and no clear evidence of intergranular fracture) [40].

Seeding sol–gel precursors with nucleation sites for growth appears to be a method of making fine-grained monolithic optically transparent materials. Initially upon heating, gels formed by mixing a colloidal boehmite–silica sol with a polymeric aluminum nitrate–TEOS sol (a hybrid type I and type II gel) tend to crystallize, forming mullite seed crystals. Homoepitactic nucleation during continued heat treatment results in mullite monoliths. The introduction of the polymeric gel resulted in an increase in apparent nucleation frequency by a factor of 1,000 at 1,375°C, and a reduction in high-temperature grain size from 1.4 to 0.4 µm at 1,550°C, with little or no intragranular porosity [41].

MacKenzie et al. [42] prepared type I gels to determine the role of preheat treatment temperature on subsequent mullite microstructure. They found that an optimal preheat temperature of about 250–350°C for a long period of time resulted in an optimal concentration of mullite in the final product. Concurrently, there was an increase in the ^{27}Al nuclear magnetic resonance spectrum at about 30 ppm. The 30 ppm Al signal is often attributed to penta-coordinated Al, which may be located in the mullite precursor

gels at the interface between Si-rich and Al-rich microdomains. MacKenzie et al. attribute this Al signal to the distorted tetrahedral Al environment in the region of O-deficient triclusters. They noted that the signal becomes increasingly strong just prior to mullitization. It was also noted that organic residues and hydroxyl groups were present up to 900°C. According to the analysis, the presence of these groups in the system at high temperatures could influence the structural evolution of the gel by providing a locally reducing and/or humid atmosphere that could facilitate tricluster formation. These sites could influence subsequent mullite formation because they form an essential element of the mullite structure. In terms of the nature of the triclusters, Schmueker and Schneider [5] proposed that the triclusters of tetrahedra may compensate the excess negative charge in the network caused by Si^{+4}–Al^{3+} substitution. Na^{+} doped into aluminosilicate gels can also compensate for the Si^{4+}–Al^{3+} substitution. For this system, the formation of triclusters was no longer required, and a significant drop in the 30 ppm Al peak was observed.

Transparent mullite may have optical applications. With a scattering loss of less than 0.01 cm^{-1}, it could be an excellent candidate for use in transparent windows in the mid-infrared range (3–5 μm wavelength). Furthermore, when mullite glass ceramics were formed with Cr^{3+} additions, significant differences in the luminescence spectra between the glassy phase and crystalline mullite were observed [43] Cr^{3+} was shown to reside in the mullite crystalline phase. The luminescence quantum efficiency increased from less than 1% to about 30% by the crystallization process. Further research is needed to establish mullite as a candidate for high-energy laser applications.

5 Selected Materials Properties

The availability of fine, pure mullite powders and novel processing routes have made it possible to obtain dense polycrystalline mullite with higher deformation resistance and hardness at higher temperatures than most other ceramics, including alumina [44,45]. Mullite has good chemical stability and a stable temperature-independent oxygen vacancy structure up to the melting point [46], making mullite particularly creep-resistant. It should be noted that the majority of studies on high temperature mechanical properties of mullite have concentrated on measurements of strength or the creep deformation under testing conditions of four point bending or compression under static loading [47,48]. These testing procedures are useful as an initial evaluation of failure strength or creep resistance but the complexity of the stress makes it difficult to interpret the effect of the material variables on the creep mechanisms [49]. Nevertheless, to cite one representative study, creep may occur by a diffusional mechanism for grain sizes <1.5 μm with stresses of less than 100 MPa at temperatures between 1,365 and 1,480°C. High activation energy of 810 kJ mol^{-1} was determined for this process. Larger grain sizes and higher stresses indicate creep occurs by slow crack growth [48]. Selected mechanical properties are provided in Table 2. In general, creep resistance increases with sintering temperature, while flexural strength decreases [50].

With a low thermal conductivity of 0.06 W cm^{-1} K^{-1} and a low thermal expansion coefficient $\alpha \sim 4.5 \times 10^{-6}°C^{-1}$, mullite is useful for many refractory applications [49]. According to Schneider, most mullites display low and nonlinear thermal expansions below, but larger and linear expansion above, ~300°C. The volume thermal expansion

Table 2 Values of fracture toughness (K_{Ic}), fracture strength (σ_f), flexural strength, and microhardness for 3:2 mullite at different temperatures

T (°C)	K_{ic} (MPa m$^{1/2}$)	σ_f (MPa)	Flexural strength (MPa)	Microhardness (GPa)
22	2.5 ± 0.5[a]			15[b]
1000				10[b]
1200	3.6 ± 0.1	260 ± 15	500[c]	
1300	3.5 ± 0.2	200 ± 20		
1400	3.3 ± 0.2	120 ± 25	360[c]	

From [49] (specimens had apparent density of 2.948 Mg m^{-3} and grain size of 4.0 μm)
[a] Value from [58]
[b] Values from [45]
[c] Values mentioned in [8]

decreases with alumina content, and the anisotropy of thermal expansion is reduced simultaneously [51].

Given that mullite is a defect structure, one would expect high ionic conductivity. Rommerskirchen et al. have found that mullite has ionic conductivity superior to that of the usual CaO-stabilized ZrO_2 solid electrolytes at temperatures from 1,400 to 1,600°C [52]. The oxygen self diffusion coefficient in the range $1{,}100 < T < 1{,}300$°C for a single crystal of 3:2 mullite has been given by [53]:

$$D_{ox} = 1.32 \times 10^{-2} \exp[-397\,\text{kJ}/RT]\,\text{cm}^2\,\text{s}^{-1} \quad (2)$$

Grain boundary diffusion coefficients are about five orders of magnitude higher than volume diffusion in the same temperature range. The activation energy for grain boundary diffusion [54] is 363 ± 25 kJ mol^{-1} – a remarkably similar value compared with that of volume diffusion.

The activation energy for silicon diffusion during the formation of mullite from fused couples at $1{,}600 < T < 1{,}800$°C [55] is in the range of $730 < \Delta H_{Si}^{4+} < 780$ kJ mol^{-1}. There is support for the idea that Al^{3+} diffusion coefficients are much higher than those of silicon at temperatures above the mullite–silica eutectic [56].

References

1. H. Schneider and K. MacKenzie, *J. Eur. Ceram. Soc*. **21**, iii (2001).
2. M. Tokonami, Y. Nakajima, and N. Morimoto, The diffraction aspect and a structural model of mullite, $Al(Al_{1+2x}Si_{1-2x})O_{5-x}$, *Acta Cryst*. **A36**, 270–276 (1980).
3. J. L. Holm, On the energetics of the mullite solid-solution formation in the system Al_2O_3–SiO_2, *J. Mat. Sci. Lett*. **21**, 1551–1553 (2002).
4. W.M. Kriven, M.H. Jilavi, D. Zhu, J.K.R. Weber, B. Cho, J. Felten, and P. C. Nordine, Synthesis and microstructure of mullite fibers grown from deeply undercooled melts, in *Ceramic Microstructures: Control at the Atomic Level*, A. P. Tomsia and A. M. Glaeser (eds.), Plenum, New York, NY, (1998) pp. 169–176.
5. M. Schmuecker and H. Schneider, Structural development of single phase (type I) mullite gels, *J. Sol–Gel Sci. Tech*. **15**, 191–199 (1999).
6. R.X. Fischer, H. Schneider, and M. Schmuecker, Crystal structure of Al-rich mullite, *Am. Mineral*., **79** (9–10), 983–990 (1994).
7. S. Freimann and S. Rahman, Refinement of the real structures of 2:1 and 3:2 mullite, *J. Eur. Ceram. Soc*. **21**, 2453–2461 (2001).

8. D.J. Cassidy, J.L. Woolfrey, and J.R. Bartlett, The effect of precursor chemistry on the crystallisation and densification of sol–gel derived mullite gels and powders, *J. Sol–Gel Sci. Tech*. **10**, 19–30 (1997).
9. I.M. Low and R. McPherson, The Origins of Mullite Formation, *J. Mat. Sci*. **24** (3), 926–936 (1989).
10. A. Kumar Chakravorty and D. Kumar Ghosh, Synthesis and 980°C phase development of some mullite gels, *J. Am. Ceram. Soc*. **71** (11), 978–87 (1988).
11. J.P. Pollinger and G.L. Messing, Metastable solid solution extension of mullite by rapid solidification, *J. Mat. Res*. **3** (2), 375–379 (1988).
12. H. Schneider and T. Rymon-Lipinski, Occurrence of pseudotetragonal mullite, *J. Am. Ceram. Soc*. **71** (3), C162–C164 (1988).
13. M. Sales and J. Alarcon, Synthesis and phase transformations of mullites obtained from SiO_2–Al_2O_3 Gels *J. Eur. Ceram. Soc*. **16**, 781–789 (1996).
14. H. Schneider, R. X. Fischer, and D. Voll, Mullite with lattice constants $a > b$, *J. Am. Ceram. Soc*. **76** (7), 1879–1881 (1993).
15. R.X. Fischer, H. Schneider, and D. Voll, Formation of aluminum rich 9:1 mullite and its transformation to low alumina mullite upon heating, *J. Eur. Ceram. Soc*. **16**, 109–13 (1996).
16. N. L. Bowen and J. W. Grieg, "The System Al_2O_3–SiO_2," *J. Am. Ceram. Soc*. **7**, 238–54 (1924).
17. E.C. Shears and W.A. Archibald, Aluminosilicate refractories, *Iron Steel* **27**, 26–30 and 61–65 (1954).
18. N.A. Toropov and F. Ya. Galakhov, Solid solutions in the system Al_2O_3–SiO_2, *Izv. Aka. Nauk SSSR Otd. Khim. Nauk* **1958**, 8 (1958).
19. S. Aramaki and R. Roy, Revised equilibrium diagram for the system Al_2O_3, *J. Am. Ceram. Soc*. **45** (5), 229–222 (1962).
20. I.A. Aksay and J. A. Pask, Stable and metastable phase equilibria in the system Al_2O_3–SiO_2, *J. Am. Ceram. Soc*. **58** (11–12), 507–512 (1975).
21. T.J. Mroz, *Microstructural Evolution of Mullite Formed by Reaction Sintering of Sol-Gels*, MS Thesis, Dept. of Cer. Eng., Alfred University, Alfred, NY, 1988.
22. J.C. Huling and G.L. Messing, Epitactic nucleation of spinel in aluminum silicate gels and effect on mullite crystallization, *J. Am. Ceram. Soc*. **74** (10), 2374–2381 (1991).
23. S. Sundaresan and I.A. Aksay, Mullitization of diphasic aluminosilicate gels, *J. Am. Ceram. Soc*. **74** (10), 2388–2392 (1991).
24. M.D. Sacks, Y.-J. Lin, G.W. Scheiffele, K. Wang, and N. Bozkurt, Effect of seeding on phase development, densification behavior, and microstructure evolution in mullite fabricated from microcomposite particles, *J Am. Ceram. Soc*. **78** (11), 2897–2906 (1995).
25. R.F. Davis and J.A. Pask, Diffusion and reaction studies in the system Al_2O_3–SiO_2, *J. Am. Ceram. Soc*. **55** (10), 525–531 (1972).
26. S.H. Risbud and J.A. Pask, Mullite crystallization from SiO_2–Al_2O_3 melts, *J. Am. Ceram. Soc*. **61** (1–2), 63–67 (1978).
27. C.G. Bergeron and S.H. Risbud, *Introduction to Phase Equilibria in Ceramics*, Am. Ceram. Soc., Columbus, OH, 1984.
28. F.J. Klug, S. Prochazka, and R.H. Doremus, Alumina–silica phase diagram in the mullite region, *J. Am. Ceram. Soc*. **70**, 750–759 (1987).
29. J.A. Pask, The Al_2O_3–SiO_2 system: logical analysis of phenomenological experimental data, in *Ceramic Microstructures: Control at the Atomic Level*, A.P. Tomsia and A.M. Glaeser (eds.), Plenum, New York, NY, 1998, pp.255–262.
30. W.E. Worrall, *Clays and Ceramic Raw Materials*, Halsted Press, New York, NY, 1975, pp. 151–152.
31. D.G. Goski and W.F. Caley, Reaction sintering of kyanite and alumina to form mullite composites, *Can. Metall. Q*. **38** (2), 119–126 (1999).
32. S. Prochazka and F.J. Klug, Infrared-transparent mullite ceramics, *J. Am. Ceram. Soc*., **66**, 874–880 (1983).
33. Y.M.M. Al-jarsha, H.G. Emblem, K. Jones, M.A. Mohd, A.B.D. Rahman, T.J. Davies, R. Wakefield, and G.K. Sargeant, Preparation, characterization and uses of mullite grain, *J. Mat. Sci*. **25** (6), 2873–2880 (1990).
34. R.D. Nixon, S. Chevacharoenkul, and R.F. Davis, Creep of hot-pressed SiC-Whisker-reinforced mullite, *Ceram. Trans*. **6**, 579–603 (1990).
35. H. Schneider, K. Okada, and J.A. Pask, *Mullite and Mullite Ceramics*, Wiley, New York, NY, 1994.

36. R.G. Chandran and K.C. Patil, A Rapid combustion process for the preparation of crystalline mullite powders, *Materi. Lett.* **10** (6), 291–295 (1990).
37. M. Schmuecker and H. Schneider, Structural development of single phase (type I) mullite gels, *J. Sol–Gel Sci. Tech*. **15**, 191–199 (1999).
38. M.J. Hyatt and N.P. Bansal, Phase transformations in xerogels of mullite composition, *J. Mat. Sci*. **25** (6), 2815–2821 (1990).
39. D.X. Li and W.J. Thomson, Mullite formation kinetics of a single-phase gel, *J. Am. Ceram. Soc*. **73** (4), 964–969 (1990).
40. P. Colomban and L. Mazerolles, SiO_2–Al_2O_3 phase diagram and mullite non-stoichiometry of sol–gel prepared monoliths: influence on mechanical properties, *J. Mat. Sci. Lett*. **9** (9), 1077–1079 (1990).
41. J.C. Huling and G.L. Messing, Hybrid gels for homoepitactic nucleation of mullite, *J. Am. Ceram. Soc*. **72** (9), 1725–1729 (1989).
42. K.J.D. MacKenzie, R.H. Meinhold, J.E. Patterson, H. Schneider, M. Schmuecker, and D. Voll, Structural evolution in gel-derived mullite precursors, *J. Eur. Ceram. Soc*. **16**, 1299–1308 (1996).
43. L.J. Andrews, G.H. Beall, and A. Lempicki, Luminescence of Cr^{3+} in mullite transparent glass ceramics, *J. Lumin*. **36** (2), 65–74 (1986).
44. P.A. Lessing, R.S. Gordon, and K.S. Mazdiyasni, Creep of polycrystalline mullite, *J. Am. Ceram. Soc*. **58** (3–4), 149–150 (1975).
45. W. Kollenberg and H. Schneider, Microhardness of mullite at temperatures to 1000°C, *J. Am. Ceram. Soc*. **72** (9), 1739–1740 (1989).
46. C. Paulmann, Study of oxygen vacancy ordering in mullite at high temperature, *Phase Trans.* **59**, 77–90 (1996).
47. T. Kumazawa, S. Ohta, H. Tabata, and S. Kanzaki, Influence of chemical composition on the mechanical properties of SiO_2–Al_2O_3 ceramics, *J. Ceram. Soc. Jpn*. **96**, 85–91 (1988).
48. Y. Okamoto, H. Fukudome, K. Hayashi, and T. Nishikawa, Creep deformation of polycrystalline mullite, *J. Eur. Ceram. Soc*. **6** (3), 161–168 (1990).
49. R. Torrecillas, J.M. Calderon, J.S. Moya, M.J. Reece, C.K.L. Davies, C. Olagnond, and G. Fantozzi, Suitability of mullite for high temperature applications, *J. Eur. Ceram. Soc*. **19**, 2519–2527 (1999).
50. H. Ohira, M.G.M.U. Ismail, Y. Yamamoto, T. Akiba, and S. Somiya, Mechanical properties of high purity mullite at elevated temperatures, *J. Eur. Ceram. Soc*. **16**, 225–229 (1996).
51. H. Schneider, "Thermal Expansion of Mullite," *J. Am. Ceram. Soc*. **73** [7] 2073–6 (1990).
52. I. Rommerskirchen, F. Cháveza, and D. Janke, Ionic conduction behaviour of mullite ($3Al_2O_3$ $2SiO_2$) at 1400 to 1600°C, *Solid State Ionics* **74** (3–4), 179–187 (1994).
53. Y. Ikuma, E. Shimada, S. Sakano, M. Oishi, M. Yokoyama, and Z.E. Nakagawa, Oxygen self-diffusion in cylindrical single-crystal mullite, *J. Electrochem. Soc*. **146** (12), 4672–4675 (1999).
54. P. Fielitz, G. Borchardt, M. Schmuecker, H. Schneider, and P. Willich, Measurement of oxygen grain boundary diffusion in mullite ceramics by SIMS depth profiling, *Appl. Surf. Sci*. **203–204**, 639–643 (2003).
55. Y.-M. Sung, Kinetics analysis of mullite formation reaction at high temperatures, *Acta Mater*. **48**, 2157–2162 (2000).
56. M.D. Sacks, K. Wang, G.W. Scheiffele, and N. Bozkurt, Effect of composition on mullitization behavior of α-alumina/silica microcomposite powders, *J. Am. Ceram. Soc*. **80** (3), 663–672 (1997).
57. B.R. Johnson, W.M. Kriven, and J. Schneider, Crystal structure development during devitrification of quenched mullite, *J. Eur. Ceram. Soc*. **21**, 2541–2562 (2001).
58. T. Huang, M.N. Rahaman, T.-I. Mah, and T.A. Parthasarathay, Anisotropic grain growth and microstructural evolution of dense mullite above 1550°C, *J. Am. Ceram. Soc*. **83** (1), 204–210 (2000).

http://www.springer.com/978-0-387-73361-6

Ceramic and Glass Materials
Structure, Properties and Processing
(Eds.)J.F. Shackelford; R.H. Doremus
2008, XII, 201 p. 67 illus., Hardcover
ISBN: 978-0-387-73361-6